

observed similarity between the dark matter and the visible densities in the Universe, i.e. $\Omega_{\text{DM}} \sim \Omega_{\text{visible}}$. The AQN construction in many respects is similar to the original quark-nugget model suggested by Witten [6], see [7] for a review. This type of DM is “cosmologically dark” not because of the weakness of the AQN interactions, but due to their small cross-section-to-mass ratio, which scales down many observable consequences of an otherwise strongly-interacting DM candidate.

There are two additional elements in the AQN model compared to the original proposal [6, 7]. First, there is an additional stabilization factor for the nuggets provided by the axion domain walls which are copiously produced during the QCD transition which help to alleviate a number of problems with the original [6, 7] nugget model. Another feature of AQN which plays absolutely crucial role for the present work is that nuggets can be made of *matter* as well as *antimatter* during the QCD transition. The direct consequence of this feature is that DM density, Ω_{DM} , and the baryonic matter density, Ω_{visible} , will automatically assume the same order of magnitude $\Omega_{\text{DM}} \sim \Omega_{\text{visible}}$ without any fine tuning as stated above. One should emphasize that AQNs are absolutely stable configurations on cosmological scales. The antimatter which is hidden in form of the very dense nuggets is unavailable for annihilation unless the AQNs hit the stars or the planets. There are also very rare events of annihilation in the center of the galaxy, which, in fact, may explain some observed galactic excess emissions in different frequency bands, see next Sect. II for references. Precisely the AQNs made of antimatter are capable to release a significant amount of energy when they enter the Earth’s atmosphere and annihilation processes start to occur between antimatter hidden in form of the AQNs and atmospheric material.

The main goal of the present work is to argue that skyquakes described above can be identified with AQN annihilation events which inevitable occur when AQNs enter the atmosphere. We support this identification by estimating the released energy, its radiation characteristics, its geometrical and time evolution. We shall argue below that all these characteristics are perfectly consistent with our identification:

$$[\text{skyquakes}] \equiv [\text{AQN annihilation events}]. \quad (1)$$

We conclude this Introduction with the following comment. The annihilation events which inevitably occur when AQN interact with environment lead to many observable effects due to release of a large amount of energy. We overview the corresponding phenomena when the annihilation events occur in the solar corona and galactic center in next section. The only comment we would like to make here is that the corresponding annihilation events when AQN enters the Earth’s atmosphere lead to the release of energy in form of the weakly coupled axions and neutrinos as well as in form of the x and γ ray radiation. It is hard to observe axions and neutrinos due to their weak interactions with material, though the cor-

responding computations have been carried out recently, see references in next section. At the same time the x and γ rays emitted by AQNs will be quickly absorbed on distances ~ 10 meters or so in the atmosphere, and therefore cannot be recovered for the analysis.

We should emphasize that there will be no visible light as a result of the AQN annihilation events. It should be contrasted with conventional meteors which typically emit visible light due to its interaction with surrounding material resulted in heating of the meteors. The visible light from conventional meteors is routinely recorded using all-sky cameras around the globe and represents an important element in identification and analysis of the events.

The analyzing of the conventional meteors and accompanying radiation plays an important role for our proposal (1). Specifically, a simultaneous recording of the infrasound signal by ELFO and non-observation of the meteors at the same time by the All-Sky and Guided Automatic and Realtime Detection (ASGARD) camera network which is synchronized with ELFO as described in [5] gives us a confidence that the recorded infrasound signal cannot be identified with conventional and much more numerous meteors. Therefore, the event [4] is a good candidate for the skyquake (1) which is the topic of Sect. IV.

Our presentation is organized as follows. In next section II we overview the AQN model in the context of the present work, paying special attention to the size distribution, frequency of appearance, energy emission pattern and other related questions. In section III we present our estimates for the AQNs propagating in atmosphere and underground. In section IV we present the arguments suggesting that the event [4] is consistent with our estimates from Section III supporting the identification (1). Finally, in Section V we present our proposal for a systematic study of such mysterious explosions originated from AQNs by employing the Distributed Acoustic Sensing which uses the optical-fiber cables. It would be very beneficial if such a fiber network is also synchronized with optical instruments which would be continuously monitoring the sky by recording the conventional meteors. This synchronization eliminates or dramatically reduces all possible spurious events.

II. AQN MODEL. THE BASICS.

The main goal of this section is to overview the basic ideas on the AQN model, its motivation, its consequences, and (yet) indirect, rather than direct, supporting observations.

The original motivation for this model can be explained in two lines as follows. It is commonly assumed that the Universe began in a symmetric state with zero global baryonic charge and later (through some baryon number violating process, non-equilibrium dynamics, and \mathcal{CP} violation effects, realizing three famous Sakharov’s criteria)

evolved into a state with a net positive baryon number.

As an alternative to this scenario we advocate a model in which “baryogenesis” is actually a charge separation (rather than charge generation) process in which the global baryon number of the universe remains zero at all times. In this model the unobserved antibaryons come to comprise the dark matter in the form of dense nuggets of antiquarks and gluons in colour superconducting (CS) phase. The result of this “charge separation” process is two populations of AQN carrying positive and negative baryon number. In other words, the AQN may be formed of either *matter* or *antimatter*. However, due to the global \mathcal{CP} violating processes associated with $\theta_0 \neq 0$ during the early formation stage, the number of nuggets and antinuggets will be different¹. This difference is always an order of one effect irrespectively to the parameters of the theory, the axion mass m_a or the initial misalignment angle θ_0 . We refer to the original papers [21–24] devoted to the specific questions related to the nugget’s formation, generation of the baryon asymmetry, and survival pattern of the nuggets during the evolution in early Universe with its unfriendly environment.

It is known that the galactic spectrum contains several excesses of diffuse emission the origin of which is not well established, and remains to be debated. The best known example is the strong galactic 511 keV line. If the nuggets have a baryon number in the $\langle B \rangle \sim 10^{25}$ range they could offer a potential explanation for several of these diffuse components. It is very nontrivial consistency check that the required $\langle B \rangle$ to explain these excesses of the galactic diffuse emission belongs to the same mass range as reviewed below. For further details see the original works [25–30] with explicit computations of the galactic radiation excesses for various frequencies, including excesses of the diffuse x- and γ - rays. In all these cases photon emission originates from the outer layer of the nuggets known as the electrosphere, and all intensities in different frequency bands are expressed in terms of a single parameter $\langle B \rangle$ such that all relative intensities are unambiguously fixed because they are determined by the Standard Model (SM) physics.

The AQNs may also offer a resolution to the so-called “Primordial Lithium Puzzle” [31], the “Solar Corona Mystery” [32, 33]. Furthermore, it may resolve [34] the longstanding puzzle with the DAMA/LIBRA observation of the annual modulation at 9.5σ confidence level, which is in direct conflict with other DM experiments if interpreted in terms of WIMP-nuclei interaction, see [35] for a short overview of the basic results of ref. [34].

The key parameter which essentially determines all the intensities for the effects mentioned above is the average

baryon charge $\langle B \rangle$ of the AQNs. There is a number of constraints on this parameter which are reviewed below. One should also mention that the AQNs masses related to their baryon charge by $M_N \simeq m_p |B|$, where we ignore small differences between the energy per baryon charge in CS and hadronic confined phases. The resulting AQN are macroscopically large objects with a typical size of $R \simeq 10^{-5}$ cm and roughly nuclear density resulting in masses roughly 10 g. For the present work we adopt a typical nuclear density of order 10^{40} cm⁻³ such that a nugget with $|B| \simeq 10^{25}$ has a typical radius $R \simeq 10^{-5}$ cm.

It should be contrasted with conventional meteors when an object with mass 10 g. would have a typical size of order 1 cm occupying the volume which would be 15 orders of magnitude larger than the AQN’s volume. This is of course due to the fact that AQNs have nuclear density which is 15 orders of magnitude higher than the density of a normal matter. One can view an AQN as very small neutron star (NS) with its nuclear density. The difference is that the NS is squeezed by the gravity, while the AQN is squeezed by the axion domain wall pressure. Precisely this drastic density difference in properties between AQNs and conventional small meteors lead to fundamentally different patterns in behaviour when they enter the Earth’s atmosphere.

We now overview the observational constraints on such kind of dense objects. The strongest direct detection limit is set by the IceCube Observatory’s, see Appendix A in [36]:

$$\langle B \rangle > 3 \cdot 10^{24} \quad [\text{direct (non)detection constraint}]. \quad (2)$$

The authors of [37] use the Apollo data to constrain the abundance of quark nuggets in the region of 10 kg to one ton. It has been argued that the contribution of such heavy nuggets must be at least an order of magnitude less than would saturate the dark matter in the solar neighbourhood [37]. Assuming that the AQNs do saturate the dark matter, the constraint [37] can be reinterpreted that at least 90% of the AQNs must have masses below 10 kg. This constraint can be approximately expressed in terms of the baryon charge:

$$\langle B \rangle \lesssim 10^{28} \quad [\text{Apollo constraint}]. \quad (3)$$

Therefore, indirect observational constraints (2) and (3) suggest that if the AQNs exist and saturate the dark matter density today, the dominant portion of them must reside in the window:

$$3 \cdot 10^{24} \lesssim \langle B \rangle \lesssim 10^{28} \quad [\text{constraints from observations}]. \quad (4)$$

We emphasize that the AQN model within window (4) is consistent with all presently available cosmological, astrophysical, satellite and ground-based constraints. This model is very rigid and predictive as there is no much flexibility nor freedom to modify any estimates mentioned above [25–34, 36]. In particular, the AQN-induced flux (6) which plays a key role in the present studies cannot change its numerical value for more than factor of 2, depending on the size distribution within the window (4).

¹ This source of strong \mathcal{CP} violation is no longer available at the present epoch as a result of the dynamics of the axion, which remains the most compelling resolution of the strong \mathcal{CP} problem, see original papers on the axion [8–10], and recent reviews [11–20].

For our interpretation of the observed mysterious event [4] as the skyquake (1) as presented in Sect. IV one needs to know the size distribution and the frequency of the appearance of the AQNs with a given size. The corresponding distribution is defined as follows: Let dN/dB be the number of AQNs which carry the baryon charge $[B, B + dB]$. The mean value of the baryon charge $\langle B \rangle$ is given by

$$\langle B \rangle = \int_{B_{\min}}^{B_{\max}} dB B f(B), \quad f(B) \propto B^{-\alpha}, \quad (5)$$

where $f(B)$ is properly normalized distribution and the $\alpha \simeq (2 - 2.5)$ is power-law index. One should note that that the algebraic scaling (5) is a generic feature of the AQN formation mechanism based on percolation theory [24], but α cannot be theoretically computed in strongly coupled QCD. Instead, the parametrization (5) is based on a proposal that the so-called nanoflares (conjectured by Parker many years ago as a mean to resolve the ‘‘Solar Corona Mystery’’) are identified with AQN annihilation events in the solar corona as discussed in [32, 33]. The main motivation for this identification is that the observed intensity of the Extreme UV emission from the solar corona nicely coincides with the total energy released as a result of the AQN annihilation events in the transition region assuming conventional value for the dark matter density around the Sun, i.e. $\rho_{\text{DM}} \simeq 0.3 \text{ GeV cm}^{-3}$. One should emphasize that this ‘‘numerical coincidence’’ is a highly nontrivial self-consistency check of the proposal [32, 33] connecting nanoflares to AQNs, since the nanoflare properties are constrained by solar corona heating models, while the intensity of the Extreme UV due to the AQN annihilation events is mostly determined by the dark matter density².

Now we estimate the AQN hitting rate assuming conventional dark matter density $\rho_{\text{DM}} \simeq 0.3 \text{ GeV cm}^{-3}$ surrounding the Earth. A full scale Monte Carlo simulations produce the following result [36]:

$$\begin{aligned} \frac{\langle \dot{N} \rangle}{4\pi R_{\oplus}^2} &\simeq \frac{4 \cdot 10^{-2}}{\text{km}^2 \text{ yr}} \left(\frac{\rho_{\text{DM}}}{0.3 \frac{\text{GeV}}{\text{cm}^3}} \right) \left(\frac{\langle v_{\text{AQN}} \rangle}{220 \frac{\text{km}}{\text{s}}} \right) \left(\frac{10^{25}}{\langle B \rangle} \right), \\ \langle \dot{N} \rangle &\simeq 0.67 \text{ s}^{-1} \left(\frac{10^{25}}{\langle B \rangle} \right) \simeq 2.1 \cdot 10^7 \text{ yr}^{-1} \left(\frac{10^{25}}{\langle B \rangle} \right), \end{aligned} \quad (6)$$

where the average over all types of AQN-trajectories with different masses $M_N \simeq m_p |B|$, with different incident angles and different initial velocities have been taken into account. The result (6) suggests that the AQNs hit the Earth’s surface with a frequency approximately once a

day per 100^2 km^2 area. The hitting rate for large size objects is suppressed by the distribution function $f(B) \propto B^{-\alpha}$ as given by (5).

It is instructive to compare the rate (6) with number of particles (collectively called meteoroids) which enter the Earth’s atmosphere every day. This rate is of order 10^8 day^{-1} , see review [38]. It is more informative to represent this daily rate number in terms of the total mass of the falling meteoroids as the AQNs are much denser objects than conventional meteoroids. The corresponding rate reads: 10^5 tons/year which is still much greater than than the total mass of order $5 \cdot 10^2 \text{ tons/year}$ associated with the dark matter AQN rate (6). Peak in size distribution for meteoroids is $2 \cdot 10^{-2} \text{ cm}$ while peak in mass is around $10 \mu\text{g}$, see [38] for review. It should be contrasted with typical size $R \simeq 10^{-5} \text{ cm}$ and masses roughly 10 g for AQNs.

The final topic to be reviewed here is the spectral properties of the AQN emission. The most important feature of the AQN spectrum which drastically distinguishes it from the conventional meteor’s emission is that the AQN spectrum is peaked in (10-50) keV range, while the optically visible bands at $\omega \sim (1 - 10) \text{ eV}$ are strongly suppressed, see Fig. 4 in Appendix A. Another crucial difference with conventional meteor’s emission is that the AQN spectrum is not a thermal black body radiation as it is originated from the annihilation events. It should be contrasted the black body radiation of conventional meteors and meteorites entering the Earth’s atmosphere with supersonic velocities and experiencing an enormous friction with the surrounding material leading to the heating of the meteoroids and surrounding material. We refer to Appendix A with short overview on spectral features of the AQNs traversing the Earth atmosphere, see in particular Fig. 4.

These features in the spectrum have some profound consequences for the present work because the AQNs do not emit the visible light, in huge contrast with conventional meteors which are normally characterized by strong emission in the visible frequency bands through sputtering and ablation [38–40]. It also implies that the AQNs cannot be observed by conventional optical monitoring as AQNs are not accompanied by emission of the visible light and cannot be routinely observed by all-sky cameras. Therefore, the observation of a signal by infrasound instruments and non-observation by the optical synchronized cameras (which must continuously monitor the sky by recording the conventional meteors) would unambiguously identify the AQNs entering the atmosphere. This synchronization eliminates or dramatically reduces all possible spurious events from sky.

² Furthermore, the required energy interval for the nanoflares must be in the range: $E_{\text{nano}} \simeq (10^{21} - 10^{26}) \text{ erg}$. This allowed interval largely overlaps with the AQN baryonic charge window given by Eq. (4) if the identification between nanoflares and AQN annihilation events is made. In this case $E_{\text{nano}} \simeq 2m_p c^2 B \simeq (3 \cdot 10^{-3} \text{ erg}) \cdot B$, see [32, 33] for the details.

III. ACOUSTIC SIGNAL FROM METEORIODS AND AQNS

A. Blast wave from meteoroids

We start by reviewing a conventional framework of the model which was designed to study meteor generated infrasound [41] (originally this model was introduced to describe a blast wave from a lightning discharge, so it has a general character). There were many recent advances and improvements of this framework including the comparison with observational data [40]. Our goal here is to use this framework to apply the basic ideas of Ref. [41] to estimate the intensity and frequency characteristics of the infrasound signal generated by AQNs propagating in the Earth's atmosphere. Our estimates cannot literally follow [40, 41] as the nature of the released energy in the case of AQN is drastically different from the energy sources associated with conventional meteors in the Earth's atmosphere. In the former case the source is the annihilation energy between atoms and molecules from the atmosphere with antimatter hidden in the AQNs, while in the later case, the energy source is friction of the meteors with the surrounding material leading to heating and radiation. However, we think that the generic scaling features describing the sound waves at large distances hold in both cases, which is precisely the key element to be used for the estimates which follow. Furthermore, the Mach number $M = v/c_s \gg 1$ (here v is the speed of the meteor and c_s is the speed of sound) is very large for meteors as well as for AQNs such that cylindrical symmetry is assumed to hold for propagating sound and infrasound waves in both cases.

The basic parameter of the approach [40, 41] is the so-called characteristic blast-wave relaxation radius defined as

$$R_0 \equiv \sqrt{\frac{E_l}{p_0}}, \quad (7)$$

where E_l is the energy deposited by the meteor per unit trail length, and p_0 is the hydrostatic atmospheric pressure. The physical meaning of this parameter R_0 is the distance at which the overpressure approximately equals the hydrostatic atmospheric pressure. In the case of a bomb-like explosion, the relevant parameter can be defined as

$$R_1 \equiv \sqrt[3]{\frac{E_{\text{point source}}}{p_0}}, \quad (8)$$

where $E_{\text{point source}}$ is the energy deposited to the air as a result of a conventional or nuclear explosion. The parameter R_1 has the same physical meaning as R_0 and it determines the distance at which the overpressure approximately equals to the hydrostatic atmospheric pressure.

In simple cases for meteors, the parameter R_0 can be directly expressed in terms of the Mach number M and

the meteor diameter d_m as $R_0 \sim M d_m$, see [40, 41]. The significance of the parameter R_0 is that the overpressure δp at larger distances can be expressed in terms of dimensionless parameter x defined as follows [40, 41]:

$$\frac{\delta p}{p_0} = \frac{2(\gamma + 1)}{\gamma} f(x), \quad x \equiv \frac{r}{R_0}, \quad f(x \gg 1) \simeq \frac{1}{x^{3/4}}, \quad (9)$$

where $\gamma = c_p/c_v$. Note that the overpressure δp decays faster than $r^{-1/2}$ as it would be for a cylindrical sound wave with a given frequency. This is due to increase of the width l of the blast wave packet as follows: $l \sim R_0 x^{1/4}$. Correspondingly, the fundamental sound frequency ν decreases as $\nu \sim c_s/l \sim (c_s/R_0) x^{-1/4}$, where c_s is the speed of sound.

The scaling (9) is justified when overpressure is relatively small. In case of conventional meteors, all parameters such as R_0 can be modelled and compared with observations [40]. We do not have such luxury in the AQN studies. However, some theoretical estimates can be made, which is precisely the topic of this section.

B. AQN in the atmosphere

We start with estimation of the parameter E_l entering (7). In the AQN framework, the energy of annihilation events occurring per unit length while the nugget traverses the atmosphere is:

$$E_l \simeq \kappa \cdot (\pi R^2) \cdot (2 \text{ GeV}) \cdot n_{\text{air}} \quad (10)$$

$$\simeq \kappa \left(\frac{10^4 \text{ J}}{m} \right) \cdot \left(\frac{B}{10^{25}} \right)^{2/3} \cdot \left(\frac{n_{\text{air}}}{10^{21} \text{ cm}^{-3}} \right),$$

where n_{air} is the total number of nucleons in atoms such that $\rho = n_{\text{air}} m_p$. The parameter κ as explained in Appendix A is introduced to account for the fact that not all matter striking the nugget will annihilate and not all of the energy released by an annihilation will be thermalized in the nuggets (for example, some portion of the energy will be released in the form of the axions and neutrinos), see the discussion after Eq. (A5). As such κ encodes a large number of complex processes including the probability that not all atoms and molecules may be able to penetrate into the colour superconducting phase of the nugget to get annihilated. It also includes complicated dynamics due to the very large Mach number $M = v_{\text{AQN}}/c_s \gg 10^2$ when shock waves are formed and the turbulence has developed. Both phenomena lead to efficient energy exchange between the nugget and surrounding material. For simplicity we keep $\kappa = 1$ in our estimates which follow.

Directly using the estimate (10), one arrives at the following approximate expression for the parameter R_0 :

$$R_0^{\text{AQN}} \equiv \sqrt{\frac{E_l}{p_0}} \sim 0.3 \left(\frac{B}{10^{25}} \right)^{\frac{1}{3}} \left(\frac{n_{\text{air}}}{10^{21} \text{ cm}^{-3}} \right)^{\frac{1}{2}} \text{ m}, \quad (11)$$

which has a physical meaning of a distance where overpressure due to the AQN annihilation events equals the hydrostatic atmospheric pressure.

Several comments are in order regarding this estimate. In the case of conventional or nuclear explosion the blast occurs as a result of the interaction of the radiation with surrounding material which rapidly heats the material. This causes vaporization of the material resulting in its rapid expansion, which eventually contributes to formation of the shock-wave. All these effects occurring in conventional explosions at very small scales, much smaller than a typical radius where over-pressure approximately equals to atmospheric pressure. In case of cylindrical symmetry the relevant parameter is determined by R_0 in Eq. (7). In case of a point-like explosion the corresponding distance R_1 is determined by (8) which plays the role of R_0 for point-like explosion.

Now we estimate the distances where the radiation is effectively converted to the shock-wave energy. In case of conventional or nuclear explosion the dominant portion of the radiation comes in the 20 eV energy range and above. At this energy, the dominant process is the atomic photoelectric effect with cross section $\sigma_{p.e.} \sim 10^7$ barn and higher such that the photon attenuation length $\lambda \sim 10^{-6}$ g/cm⁻², see e.g. Fig. 33.15 and Fig. 33.16 in [42] and references therein. In case of meteoroids the emission normally occurs in (1–20) eV energy range, which also includes the visible light emission. These spectrum features in air imply that the energy due to the heating will be completely absorbed on the scales which are much shorter than R_0 defined by (7), i.e.

$$\frac{\lambda}{\rho_{\text{air}}} \lesssim 10^{-3} \text{ cm} \ll R_0 \quad [\text{meteoroids}]. \quad (12)$$

This should be contrasted with the AQN case with a drastically different radiation spectrum with typical energy in the ~ 40 keV range as reviewed in Appendix A. In this case the atomic photoelectric effect which is still the dominant process and the photon attenuation length is $\lambda \sim 0.5$ g/cm⁻² such that

$$L = \frac{\lambda}{\rho_{\text{air}}} \sim 5 \text{ m} \gg R_0^{\text{AQN}} \quad [\text{AQN events}]. \quad (13)$$

These estimates suggest that only a small portion of the energy (10) will be released in the form of a blast, while the rest of the energy will simply heat the surrounding material. The attenuation length is even longer for higher-energy photons which saturate the total intensity for $T_{\text{AQN}} \simeq 40$ keV, see Appendix A.

We can do an estimate of overpressure in this case as follows. The annihilation energy $E_l z$ released on the track of the length z is absorbed in the volume of the cylinder $V = \pi L^2 z$. The internal energy of a diatomic ideal gas (air) is given by $U = (5/2)PV$. This gives an estimate of overpressure inside this volume V :

$$\delta p_0 \approx \frac{E_l}{2.5\pi L^2} \quad [\text{AQN events}]. \quad (14)$$

As explained above, outside this volume, δp decreases as $f(\bar{x}) \approx \bar{x}^{-3/4}$, where we introduced the dimensionless parameter $\bar{x} = r/L$, which plays the same role as x in meteoroids formula (9):

$$\delta p(r) \approx \frac{\delta p_0}{\bar{x}^{3/4}} \approx \frac{E_l}{2.5\pi L^2} \left(\frac{1}{\bar{x}}\right)^{3/4} \quad [\text{AQN events}]. \quad (15)$$

To illustrate the significance of the estimate (15), we present an order of magnitude numerical estimate for the overpressure at a distance r , with the annihilation energy given by Eq. (10) and absorption of this energy within the radius $L = 5$ m as estimated by (13):

$$\delta p \approx 0.03 \text{ Pa} \left(\frac{B}{10^{25}}\right)^{2/3} \left(\frac{100 \text{ km}}{r}\right)^{3/4} \quad [\text{AQN events}]. \quad (16)$$

This estimate shows that a typical AQN generates very small overpressure $\delta p/p \sim 10^{-3}$ even inside the absorption region $r \lesssim L$, which should be contrasted with the meteoroid case (9) where $\delta p/p \approx 1$ at $r \simeq R_0$. The difference is due to the large length $L \simeq 5$ m in comparison with the small absorption distance $\sim 10^{-3}$ cm for the meteoroids (12). The temperature increase in surrounding region $\delta T/T \sim \delta p/p \sim 10^{-3} \ll 1$ is too small to produce visible thermal radiation around the AQN path.³

Another important characteristic of the acoustic waves produced by meteoroids is the scaling behaviour of the so called line-source wave period $\tau(x)$ at large distances. The scaling behaviour can be expressed in terms of the same dimensionless parameter x introduced above, and it is given by [40, 41]:

$$\tau(x) \simeq 0.562\tau_0 x^{1/4}, \quad \tau_0 = 2.81 \frac{R_0}{c_s} \quad [\text{meteoroids}], \quad (17)$$

where τ_0 is the so-called fundamental period where numerical factors 2.81 and 0.562 in Eq. (17) have been fitted from the observations [40]. Equation (17) determines the frequency of the sound (infrasound) wave at a distant point x :

$$\nu(x) \equiv \tau^{-1}(x) \sim \tau_0^{-1} x^{-1/4}, \quad x \gg 1 [\text{meteoroids}]. \quad (18)$$

The same scaling behaviour is expected to hold for the AQN case. However, the parameters for AQNs are different:

$$\tau_0 \sim \frac{L}{c_s}, \quad \tau(\bar{x}) \sim \tau_0 \bar{x}^{1/4}, \quad \nu_0 \equiv \frac{1}{\tau_0} \sim 70 \text{ Hz}, \quad (19)$$

where we ignore all numerical factors which in the case of meteoroids were fixed by matching with observations, and obviously cannot be applied to our present studies of the AQNs. In this case we arrive at the following estimate for the frequency at a distance r :

$$\nu(\bar{x}) \sim \frac{\nu_0}{\bar{x}^{1/4}} \sim 6 \text{ Hz} \left(\frac{100 \text{ km}}{r}\right)^{1/4} \quad [\text{AQN events}]. \quad (20)$$

³ This temperature should not be confused with the much higher internal AQN temperature $T_{\text{AQN}} \sim 10$ keV.

Thus, at a large distance from the AQN track in the air there will be emission of the infrasound waves of low frequency. We will see below that for the signal from an underground AQN track, the overpressure and the frequency are both several orders of magnitude higher.

C. AQN in underground

One should emphasize that the infrasound waves originating from AQNs as estimated in Sec. III B will be always accompanied by sound waves emitted by the same AQNs when the nuggets hit the Earth surface and continue to propagate in the deep underground. The corresponding estimates of intensity and frequency of the sound emitted as a result of the annihilation events occurring underground are presented in this subsection.

The starting point is similar to (10) which for underground rocks assumes the form:

$$E_i^\downarrow \simeq \kappa \cdot (\pi R^2) \cdot (2 \text{ GeV}) \cdot n_{\text{rock}} \quad (21)$$

$$\simeq \kappa \left(\frac{10^7 \text{ J}}{m} \right) \cdot \left(\frac{B}{10^{25}} \right)^{2/3} \cdot \left(\frac{n_{\text{rock}}}{10^{24} \text{ cm}^{-3}} \right),$$

where we use the notation E_i^\downarrow for the energy produced by annihilation (some of which may remain in the AQN) to avoid confusion with the similar equation (10) applied to the atmosphere, n_{rock} is the total number of nucleons in atoms such that $\rho = n_{\text{rock}} m_p$.

We introduce an unknown parameter ξ^\downarrow which applies to the underground case (at sufficiently high density of the surrounding material) to account for the complicated physics which describes the transfer of the AQN energy into the the surrounding material energy denoted as $E_{\text{blast}}^\downarrow$:

$$E_{\text{blast}}^\downarrow = \xi^\downarrow \cdot \left(\frac{10^7 \text{ J}}{m} \right) \cdot \left(\frac{B}{10^{25}} \right)^{2/3} \cdot \left(\frac{n_{\text{rock}}}{10^{24} \text{ cm}^{-3}} \right). \quad (22)$$

There are several important new elements in comparison with the atmospheric case discussed in Sec. III B. First of all, the increase of the density of the surrounding material naively drastically increases the released annihilation energy as Eq. (21) suggests assuming that the coefficient κ remains the same as in the atmospheric case, Eq. (10). However, it is expected that this assumption is strongly violated.⁴ If one removes the low-energy

positrons from the electrosphere, the suppression factor could be $\xi^\downarrow \sim 10^{-2}$ and even much smaller.⁵

The most important effect which was ignored in the atmosphere in Sec. III B is that δp could be much larger underground in comparison with the estimate of Eq. (16). It results in pushing material from the AQN path which effectively decreases the geometrical cross section πR^2 assumed in (21). This effect further suppresses the parameter ξ^\downarrow entering (22).

We cannot at the moment compute ξ^\downarrow from first principles as mentioned in footnotes 4 and 5. Therefore, we keep it as a phenomenological unknown parameter which strongly depends on the environment, temperature T_{AQN} and many complex processes as mentioned above.

Another important parameter is the absorption length $L^\downarrow(T_{\text{AQN}})$ for the energy emitted by AQN in underground (hence the \downarrow label), which also indirectly depends on the AQN internal temperature T_{AQN} . This is because the length L^\downarrow strongly depends on the energy of the photons emitted by the AQNs, which is determined by the internal temperature T_{AQN} . For the photon energy $\sim 100 \text{ keV}$, an absorption length in silicon is about $L^\downarrow \simeq 2 \text{ cm}$. However, it is an order of magnitude larger for 1 MeV photons. We account for this uncertainty by introducing another unknown dimensionless parameter η defined as follows: $L^\downarrow(T_{\text{AQN}}) = (2 \text{ cm}) \cdot \eta$. In terms of these unknown parameters the deposited energy per unit volume ϵ_{blast} surrounding the AQN can be estimated as follows:

$$\epsilon_{\text{blast}} \simeq 10^2 \frac{\text{J}}{\text{cm}^3} \cdot \left(\frac{\xi^\downarrow}{10^{-2}} \right) \cdot \left(\frac{1}{\eta^2} \right),$$

which leads to an instantaneous increase of temperature ΔT of the surrounding material:

$$\Delta T \simeq 30 \text{ K} \cdot \left(\frac{\xi^\downarrow}{10^{-2}} \right) \cdot \left(\frac{1}{\eta^2} \right). \quad (23)$$

We now in position to estimate the overpressure for the blast wave in two different approximations. First, we may estimate the overpressure as deposited energy per unit volume. This yields

$$\delta p \simeq 10^7 \text{ Pa} \cdot \left(\frac{\xi^\downarrow}{10^{-2}} \right) \cdot \left(\frac{1}{\eta^2} \right) \text{ at } r \simeq L^\downarrow. \quad (24)$$

Another approximation is based on an increase of pressure due to the thermal expansion of solids. Relative thermal expansion of silicon is $\delta x/x = 2.6 \cdot 10^{-6} / \text{K}$, the

⁴ The main reason for that is due to increase of the internal temperature T_{AQN} which consequently leads to strong ionization of the positrons from electrosphere. As a result of this ionization the positron density of the electrosphere (which is responsible for the emissivity) drastically decreases. It suppress the emissivity from the electrosphere as Eq. (A1) states. It should be contrasted with the BB radiation where emissivity scales as $\sim T^4$. In our case, the source of emission are the positrons from electrosphere, not BB radiation.

⁵ Such simplified procedure for the estimate of ξ^\downarrow by complete removing the low energy states is not a proper way of computation because the positron's density will be adjusting when T_{AQN} varies. The consistent procedure would be a mean-field computation of the positron density by imposing the proper boundary conditions relevant for nonzero temperature and non-zero charge, similar to $T_{\text{AQN}} \approx 0$ computations carried out in [29, 30]. The corresponding computations have not been done yet, and we keep the parameter $\xi^\downarrow(T_{\text{AQN}})$ as a phenomenological free parameter.

Young modulus is $150 \text{ GPa} \sim 10^{11} \text{ Pa}$. This gives the same order of magnitude as in the dimensional estimate (24).

Our next task is to estimate the amplitude of the wave at large distance r . Using the conventional scaling arguments when $\delta p(r) \sim 1/(\bar{x}^\downarrow)^{3/4}$ with dimensionless parameter \bar{x}^\downarrow defined as $\bar{x}^\downarrow = r/L^\downarrow$ we arrive to the following estimate for overpressure at a distance r :

$$\delta p(r) \sim 10^2 \cdot \left(\frac{\xi^\downarrow}{10^{-2}}\right) \cdot \left(\frac{1}{\eta}\right)^{\frac{5}{4}} \cdot \left(\frac{100 \text{ km}}{r}\right)^{\frac{3}{4}} \text{ Pa.} \quad (25)$$

Following the same logic as for Eq. (20) we obtain a numerical estimate for the frequency of sound emitted by an AQN propagating underground:

$$\tau_0 \sim \frac{L^\downarrow}{c_s}, \quad \tau(\bar{x}^\downarrow) \sim \tau_0 \cdot \sqrt[4]{\bar{x}^\downarrow}, \quad \nu_0 \equiv \frac{1}{\tau_0} \simeq 170 \left(\frac{1}{\eta}\right) \text{ kHz,}$$

where we use $c_s \simeq 3 \text{ km/s}$ for speed of sound in rocks. For large distances r our estimate for the frequency becomes

$$\nu(\bar{x}^\downarrow) \sim \frac{\nu_0}{\sqrt[4]{\bar{x}^\downarrow}} \sim 3.5 \left(\frac{1}{\eta}\right)^{\frac{3}{4}} \cdot \left(\frac{100 \text{ km}}{r}\right)^{\frac{1}{4}} \text{ kHz,} \quad (26)$$

which is almost three orders of magnitude higher than the frequency of the infrasound emitted by AQNs in atmosphere (20).

In the estimate (25) above we assumed that the absorption can be neglected⁶. We now estimate the corresponding attenuation effects to support our assumption. To proceed with estimates we note that the sound absorption length scales as $\propto \nu^{-2}$. A proper estimation of the absorption effects must include the integration over distance where sound wave propagates since the frequency depends on the distance according to (26) as $\nu \propto r^{-1/4}$ and the absorption length $l \propto \nu^{-2} \propto r^{1/2}$. As a result, formula (25) will receive an additional exponential factor which describes the suppression of the sound intensity (intensity $\propto \delta p^2$) due to the absorption of the sound wave:

$$\exp(-X), \quad \text{where} \quad X \approx 2 \frac{[L^\downarrow r]^{\frac{1}{2}}}{l_0 \eta^2}, \quad (27)$$

where l_0 is the absorption length for the initial frequency ν_0 . For a numerical estimate of the blast wave absorption we may use detailed data on the sound absorption in sea water [47]. The absorption length for sound with $\nu_0 \simeq 170 \text{ kHz}$ is $l_0 \simeq 0.1 \text{ km}$, and we arrive at an estimate for $X \simeq \eta^{-3/2}$ for $r = 100 \text{ km}$. Since η is probably larger than 1, this gives us an indication that a significant part

of the blast wave may reach a detector on the distance up to 100 km.

The absorption of the blast wave is even smaller in water where the sound frequency is expected to be significantly smaller. For the photon energy $\sim 100 \text{ keV}$ the absorption length in water is 4.15 cm, so we assume $L^\downarrow = 4.15\eta \text{ cm}$. The speed of sound in water is $c_s = 1.5 \text{ km/s}$, so we have our estimate for frequency in water $\nu_0 \simeq 36 \text{ kHz}$ and

$$\nu(\bar{x}^\downarrow) \sim \frac{\nu_0}{\sqrt[4]{\bar{x}^\downarrow}} \sim \left(\frac{1}{\eta}\right)^{\frac{3}{4}} \cdot \left(\frac{100 \text{ km}}{r}\right)^{\frac{1}{4}} \text{ kHz.} \quad (28)$$

The sound absorption length in water is $l_0 \simeq 0.45 \text{ km}$ and $X \simeq 0.2\eta^{-3/2}$ for $r = 100 \text{ km}$. Thus, the absorption of the blast wave in water is insignificant.

We conclude this section with the following comment. In case of conventional meteoroids all numerical factors entering the scaling relations such as (9) and (17) have been fitted to match with numerous observations. Therefore, we introduce into our AQN estimates empirical parameters ξ^\downarrow and η which are very hard to compute from the first principles, but could be fixed by observations. Further studies are needed to collect more statistics of mysterious events when sound signatures are recorded without any traces in the synchronized optical monitoring systems. In the next section we present several arguments to support our identification (1) based on the ELFO infrasonic record.

IV. THEORY CONFRONTS THE OBSERVATIONS

Our goal here is to present several arguments suggesting that the mysterious explosion which occurred on July 31st 2008 and which was properly recorded by dedicated Elginfield Infrasound Array (see [43] [44] for a short description) might be a good candidate supporting our identification (1) between mysterious skyquakes and the AQN annihilation events. Localization of the source position, Elginfield Infrasound Array (ELFO) and seismic stations are shown on Fig.1 adopted from [4].

The sounds, as reported by residents of Kincardine, Ontario, Canada were apparently loud enough to rattle windows and objects on walls. An important point here is that the infrasound detection associated with this sound shock was recorded by ELFO as presented in Fig. 2 with a typical overpressure $\delta p \sim 0.3 \text{ Pa}$. These observations (along with non-observations in the all-sky camera network [45]) ruled out a meteor source, as well as operations at the Bruce Nuclear Power Plant, while Goderich salt mine logs eliminated it as a source [4]. Furthermore, a local airport radar reported no aircraft in the area at the time. The impulses were also observed seismically as ground coupled acoustic waves around South Western Ontario and Northern Michigan as shown on Fig. 3.

Now we are in a position to apply the scaling behaviour (16) to see if the mysterious event recorded by ELFO

⁶ In analogous estimate studied in previous Section III B for the infrasound produced by AQN in the air this assumption is well-justified. One can easily convince yourself that the estimate (16) is practically unaffected by absorption on the distance well above 100 km.

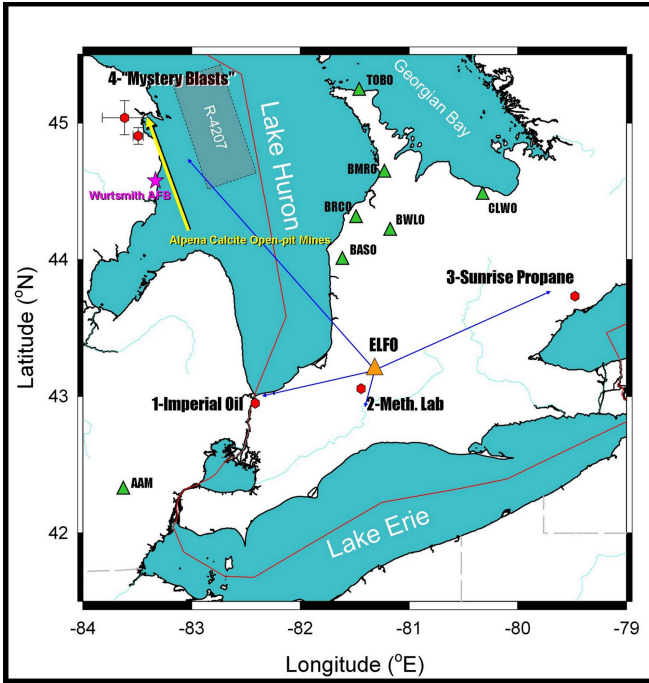


FIG. 1. Location of ELFO and seismic stations in the area, adopted from [4]. One degree along the latitude corresponds to 112 km. i.e. $1^\circ \approx 112$ km, while along the longitude $1^\circ \approx 82$ km. It explains our benchmark 300 km in eqs. (29) and (30) which covers the relevant area shown on the map.

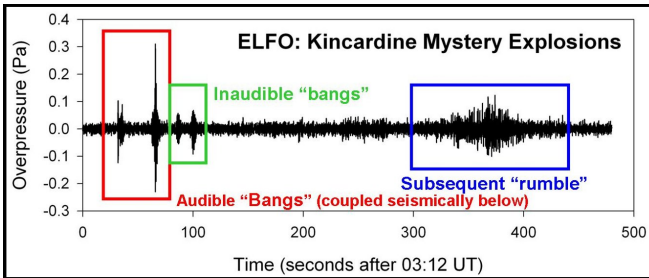


FIG. 2. Infrasound impulses as recorded by ELFO, adopted from [4].

might have resulted from the AQN annihilation events along its trajectory when it crosses the atmosphere in this area. Our estimate (16) suggests that the overpressure δp assumes the following numerical value at $r \simeq 300$ km:

$$\delta p \approx 0.3 \text{ Pa} \left(\frac{B}{10^{27}} \right)^{2/3} \left(\frac{300 \text{ km}}{r} \right)^{3/4}, \quad (29)$$

where we choose the benchmark for $r = 300$ km corresponding to a typical distances in the area shown on Fig. 1, and $B = 10^{27}$ to bring the numerical coefficient close to the measured value $\delta p \simeq 0.3$ Pa as recorded by ELFO, see Fig. 2. Estimation for the intensity (29) is consistent with observation $\delta p \simeq 0.3$ Pa if one assumes that the mysterious explosion had resulted from the AQN annihilation event of a relatively large size with the baryon

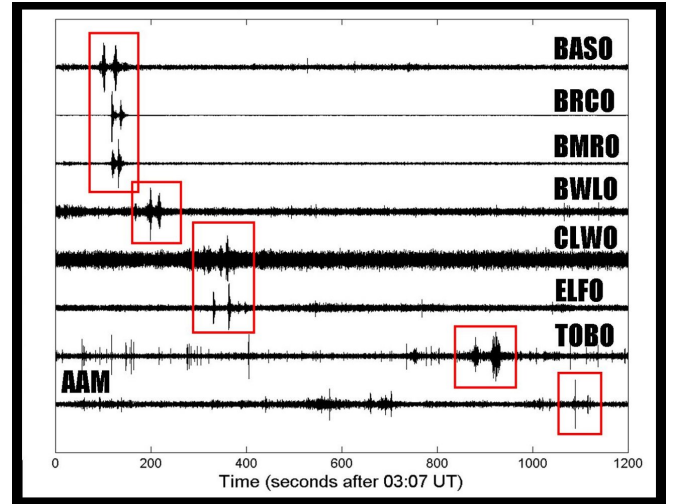


FIG. 3. Impulses as observed by seismic stations in the area, adopted from [4].

charge $B \simeq 10^{27}$. We shall support this interpretation at the end of this section by analysing the frequency of appearance of such large sized nuggets.

Another parameter which characterizes the acoustic shock is the frequency determined by the scaling formula (20). Assuming the same numerical parameters as before we arrive at the following numerical estimate:

$$\nu(\bar{x}) \sim \frac{\nu_0}{\bar{x}^{1/4}} \sim 5 \text{ Hz} \left(\frac{300 \text{ km}}{r} \right)^{1/4}, \quad (30)$$

which is precisely in the range of the highest sensitivity of ELFO where the noise levels are: $10^{-4} \text{ Pa}^2/\text{Hz}$ for the 10 Hz frequency band and $10^{-3} \text{ Pa}^2/\text{Hz}$ in the 1 Hz frequency band [43, 44].

Now our task is to estimate the relevant frequency for the sound emitted in the underground rocks. The corresponding expression for the frequency at $r \simeq 300$ km is determined by the scaling relation (26) and it is given by:

$$\nu(\bar{x}^\perp) \sim \frac{\nu_0}{\sqrt[4]{\bar{x}^\perp}} \sim 2.5 \left(\frac{1}{\eta} \right)^{3/4} \cdot \left(\frac{300 \text{ km}}{r} \right)^{1/4} \text{ kHz}. \quad (31)$$

The estimate for the underground frequency of Eq. (31) should be contrasted with the estimate of Eq. (30) for the atmosphere. The basic observation is that the acoustic waves in the atmosphere are in the infrasonic frequency range, while underground, they are in the sound frequency band, as already mentioned.

Several comments are in order. First of all, our proposal demonstrates a qualitative consistency with the mysterious event recorded by ELFO on July 31st 2008. Indeed, as we mentioned above the AQNs do not emit directly the visible light, see Appendix 4. It should be contrasted with conventional meteors which directly emit the visible light being consistent with black body radiation spectrum. This observation implies that the AQNs

cannot be observed by conventional optical monitoring. The mysterious event recorded by ELFO on July 31st falls into this category because it was observed by infrasound instruments and not observed by the optical synchronized cameras.

Furthermore, our estimations are consistent with the mysterious event recorded by ELFO on July 31st 2008, on the quantitative level as our estimates for overpressure (29) and the frequency estimate (30) are consistent with description [4] represented on Fig. 2. This obviously should be considered as a strong support of our identification (1) between AQN events and skyquakes.

Our next comment goes as follows. The frequency (31) of the sound from the underground blast falls in human hearing range. Therefore, it is also consistent with the fact that residents of nearby Kincardine could hear the sound (rather than infrasound) signal which originates from the underground with frequency (31). It is also consistent with seismic observations which are correlated⁷ with infrasound impulses recorded by ELFO. As discussed above, the atmospheric and underground acoustic waves emitted by the same AQN are always accompanied by each other as they originate from one and the same AQN propagating from outer space through the atmosphere and the Earth.

We also comment on a different event that happened in Alabama sky in 2017 when the sound was heard across 15 counties. There were no related meteor-activity reports. There were, however, reports of *vapor* trails [46]. Our original comment here is that the presence of the *vapor* is expected and in fact predicted by the proposal (1) because most of the released energy (10) will heat the surrounding material, while a small portion of the energy will be released in the form of the sound (infrasound) waves as explained in the text. There will be no significant emission in visible bands. Therefore, it is not a surprise that there were no reports on meteor activity in that event but there were reports of *vapor* trails [46].

Our final comment is related to the energetics and frequency of appearance of such mysterious events interpreted in terms of the AQNs. We think that a relatively high overpressure (29) at the level of $\delta p \simeq 0.3$ Pa is due to sufficiently large AQN with $B \simeq 10^{27}$ to be compared with average nugget size $\langle B \rangle \simeq 10^{25}$. The radius of the nuggets goes as $R \sim B^{1/3}$ which effectively leads to an increase in the number of annihilation events for larger nuggets, which eventually releases higher energy output per unit length as Eq. (10) states. Such events with large $B \simeq 10^{27}$ are relatively rare according to (6) and (5) as the frequency of appearance is proportional to $f(B) \sim B^{-\alpha}$ with $\alpha \simeq (2 - 2.5)$. It might be a part of an explanation of why this area has observed a single event in 10 years rather than observing similar events much more often.

⁷ The corresponding bangs are classified as seismically coupled “Audible Bangs”.

We conclude this section as follows. We argued that a single mysterious event properly recorded by ELFO on July 31st 2008 supports our proposal on identification (1) between dark matter AQN events and skyquakes. We need much more statistics to convincingly support this identification. In the next section we present a possible design of an instrument which could be sufficiently sensitive to infrasound signals such that much smaller (than mysterious event recorded by ELFO on July 31st 2008) but much more frequent events with $B \simeq 10^{25}$ could be recorded. In this case, we can systematically record a large number of such events which manifest themselves in the form of the infrasonic signals, while the optical synchronized cameras may not see any light from these events. Infrasonic signals must be always accompanied by sound waves as discussed above, and which can be routinely recorded by conventional seismic stations, similar to the ones presented on Fig. 3. These events should demonstrate the daily and annual modulations as the source for these events is the dark matter galactic wind.

V. DETECTION STRATEGY AND POSSIBLE INSTRUMENTS

We argued in Sec. IV that a single mysterious event properly recorded by ELFO on July 31st 2008 can be explained as a result of a rare event of the AQN hitting the Earth surface. We estimated that the size of the nugget must be sufficiently large $B \simeq 10^{27}$ to produce a strong signal $\delta p \simeq 0.3$ Pa as observed by ELFO. Such large nuggets are very rare events as the frequency of appearance is proportional to $f(B) \sim B^{-\alpha}$ with $\alpha \simeq (2 - 2.5)$. Small nuggets with $B \sim 10^{25}$ are much more common events, but generate much weaker signal. The sensitivity of the instruments similar to ELFO is not sufficient to record relatively small events in the atmosphere which occur approximately once a day in an area of $(100 \text{ km})^2$ with $\delta p \simeq 0.01$ Pa and frequency $\nu \simeq 5$ Hz.

We would like to have a systematic study of such events, in contrast with random observations such as the single event presented in the previous section. In this section we suggest several possible designs of instruments which we think are capable of fulfilling this role as sufficiently sensitive devices to detect the dark matter signals from small and common AQNs with $B \sim 10^{25}$.

We start the overview with a promising recent development, Distributed Acoustic Sensing (DAS), which is becoming a conventional tool for seismic and other applications, see, for example, [48–51] and references therein. The basic idea of these activities can be explained as follows. It has been known for quite sometime that distributed optical fiber sensors are capable of measuring the signals at thousands of points simultaneously using an unmodified optical fiber as the sensing element. The recent development is that the DAS is capable of measuring strain changes at all points along the optical fiber at *acoustic frequencies*, which is crucial for our studies of

the acoustic waves emitted due to the AQN passage.

The main element of the DAS technology is that a pulse of light is sent into optical fiber and, through scattering in the glass, a small amount of the incident light is scattered back towards the sensing unit. The key point is that the DAS is capable of determining from this scattered light, a component which indicates changes in the local axial strain along the fibre. It has been shown that this technology is capable of detecting signals at frequencies as low as 8 mHz and as high as 49.5 kHz with sensitivity at the level of $\delta p \sim 0.1 \text{ mBar} \approx 10 \text{ Pa}$ [48] which is more than sufficient for our purposes for δp as estimated in (25) and typical frequencies in kHz band as estimated in (26). Furthermore, it has been shown that using an amplifier chain one can extend the range of DAS unit to 82 km, while maintaining high signal quality [48]. Such a long range on the scale of 100 km matches well with what is needed for AQN-passage detection. Indeed, we anticipate approximately one event per day per an area of $(100 \text{ km})^2$ according to (6) reviewed in Section II. An important point is that such studies can in principle detect not only the intensity and the frequency of the sound wave, but also the direction of the source. We note that networks of optical-fiber telecommunication cables cover a significant part of the Earth's surface.

We anticipate that the main problem with DAS will be separation of the AQN signal from the seismic noise and numerous spurious events. We discuss one of the possibilities to separate the signal from a much larger noise below. The main point is that the AQN signal must show the annual (32) and daily (33) modulations characteristic of the dark matter galactic wind, in contrast with much more numerous and much more intense random events. One of possibilities to separate the signal from a much larger noise was suggested in [52].

The basic idea of [52] can be explained as follows. The AQN flux is given by (6) if averaged over very long period of time, longer than a year. However, due to the relative motion and orientation of the Sun, Earth and the galaxy, the AQN flux, as that of any other dark matter particle, receives the time-dependent factor $A_{(a)}(t)$ representing the annual modulation which is defined as follows:

$$A_{(a)}(t) \equiv [1 + \kappa_{(a)} \cos \Omega_a(t - t_0)], \quad (32)$$

where $\Omega_a = 2\pi \text{ yr}^{-1} \approx 2\pi \cdot 32 \text{ nHz}$ is the angular frequency of the annual modulation and label “a” in Ω_a stands for annual. The $\Omega_a t_0$ is the phase shift corresponding to the maximum on June 1 and minimum on December 1 for the standard galactic DM distribution, see [53, 54]. Similar daily modulations are also known to occur [55] and can be represented as follows:

$$A_{(d)}(t) \equiv [1 + \kappa_{(d)} \cos(\Omega_d t - \phi_0)], \quad (33)$$

where $\Omega_d = 2\pi \text{ day}^{-1} \approx 2\pi \cdot 11.6 \mu\text{Hz}$ is the angular frequency of the daily modulation, while ϕ_0 is the phase shift similar to $\Omega_a t_0$ in (32). It can be assumed to be constant on the scale of days. However, it actually slowly

changes with time due to the variation of the direction of DM wind with respect to the Earth. The modulation coefficients $\kappa_{(a)}$ and $\kappa_{(d)}$ have been computed in the AQN model in [55] and numerically both around 10%.

The idea advocated in [52] is to fit the data to the modulation formulae (32) and (33) even if the noise is large and exceeds the expected signal. The key point here is the statistics factor and accumulation of the signal for a long period of time assuming that the noise can be treated as being random in contrast with signal being characterized by well defined frequencies Ω_a and Ω_d . A hope is to discover the annual (32) and daily (33) modulations by recording a large number of AQN events which represent the dark matter galactic wind in this specific model.

A specific signal from AQN tracks is very different from the ordinary seismic noise and earthquakes. Therefore, AQN signals may, in principle, be detected by an existing network of seismic stations.

We would like to briefly mention other possibilities for the AQN detection, see also relevant references in Section II leading to the constraints (4). The AQN produce only a small amount of visible light as we already mentioned. However, the emitted x-rays will be absorbed and heat the atmosphere along the track on scales of order L as Eq. (13) suggests. It may produce vapor tracks along the AQN path as reported in [46]. Therefore, one may try to observe infrared radiation from AQN tracks using infrared telescopes being synchronized with infrasonic detectors and all-sky cameras. Similarly, the AQN tracks also produce microwave and radio wave radiation which may be detected by radio telescopes which can be also synchronized with infrasonic and all sky cameras.

In addition to optical-fiber based methods, it may be possible to search for the AQN-passage signatures also in the large volumes of existing historical data from networks of seismometers [56].

Finally, while an AQN itself is only $R \simeq 10^{-5} \text{ cm}$ in size, nevertheless, it may leave larger and noticeable cracks along its path in solids as instantaneous defect creation and temperature increase occur on a cm scale according to (23). The cracks could be sufficiently large to be observed. A search for AQN annihilation tracks could also be performed in old rocks and Antarctic ice.

VI. CONCLUSION

The main results of the present work can be summarized as follows:

1. We argue that the mysterious explosion which occurred on July 31st 2008 and which was properly recorded by the dedicated Elginfield Infrasound Array [43, 44] might be a good candidate supporting our identification (1) between mysterious skyquakes and the AQN annihilation events;
2. Our proposal successfully passed a number of consistency checks (such as non-observation of a signal in the

visible, which normally accompanies conventional meteoroids) as discussed at the end of Section IV;

3. Our basic estimates for the overpressure (29) and the frequency (30) are amazingly close to the signal recorded by ELFO. One should emphasize that our estimates were based on parameters of the AQN model which were fixed long ago for completely different purposes in very different occurrences in drastically different environment as reviewed in Section II. By no means we fitted our parameters to accommodate the observed ELFO mysterious signal;

4. We propose a detection strategy to search for a signal by using Distributed Acoustic Sensing as discussed in Section V. Specific signals from AQN passage may also be detected with a variety of alternative techniques, for instance, with an existing network of seismic stations (or even by analyzing the already existing data).

The estimates are based on the AQN model. Why should one take this model seriously? A simple answer is as follows. Originally, this model was invented to explain the observed relation $\Omega_{\text{DM}} \sim \Omega_{\text{visible}}$ where the “baryogenesis” framework is replaced with a “charge-separation” paradigm, as reviewed in the Introduction. This model is shown to be consistent with all available cosmological, astrophysical, satellite and ground-based constraints, where AQNs could leave a detectable electromagnetic signature as reviewed in the Introduction, with one and the *same set* of parameters. Furthermore, it has been also shown that the AQNs could be formed and could survive the early Universe’s unfriendly environment. Therefore, the AQNs are entitled to serve as the DM candidates by all standards. Finally, the same AQN framework may also explain a number of other (naively unrelated) observed phenomena such as excess of the galactic diffuse emission in different frequency bands, the so-called “Primordial Lithium Puzzle”, “The Solar Corona Mystery”, and the DAMA/LIBRA puzzling annual modulation, see Section II for the references.

Our identification (1) between mysterious skyquakes and the AQN annihilation events, if confirmed by future studies, would be the *first direct* (non-gravitation) evidence which reveals the nature of the DM, in contrast with *indirect* observations mentioned above.

ACKNOWLEDGMENTS

The authors are grateful to Mark G. Raizen, Vincent Dumont, Nataniel Figueroa Leigh and Jonathan B. Ajo-Franklin for the discussion of fiber-networks for acoustic detection. The work of DB was supported in part by the DFG Project ID 390831469: EXC 2118 (PRISMA+ Cluster of Excellence). DB also received support from the European Research Council (ERC) under the European Union Horizon 2020 Research and Innovation Program (grant agreement No. 695405), from the DFG Reinhart Koselleck Project and the Heising-Simons Foundation. The work of VF is supported by the Australian Research

Council, the Gutenberg Fellowship and the New Zealand Institute for Advanced Study. The work of AZ was supported in part by the National Science and Engineering Research Council of Canada.

Appendix A: AQN emission spectrum

The goal of this Appendix is to overview the spectral characteristics of the AQNs as a result of annihilation events when the nugget enters the Earth atmosphere. The corresponding computations have been carried out in [29] in application to the galactic environment with a typical density of surrounding visible baryons of order $n_{\text{galaxy}} \sim 300 \text{ cm}^{-3}$ in the galactic center. We review these computations with few additional elements which must be implemented for Earth’s atmosphere when typical density of surrounding baryons is much higher $n_{\text{air}} \sim 10^{21} \text{ cm}^{-3}$.

The spectrum of nuggets at low temperatures was analyzed in [29] and was found to be,

$$\begin{aligned} \frac{dF}{d\omega}(\omega) &= \frac{dE}{dt dA d\omega} \simeq \frac{1}{2} \int_0^\infty dz \frac{dQ}{d\omega}(\omega, z) \sim \\ &\sim \frac{4}{45} \frac{T^3 \alpha^{5/2}}{\pi} \sqrt[4]{\frac{T}{m}} \left(1 + \frac{\omega}{T}\right) e^{-\omega/T} h\left(\frac{\omega}{T}\right), \quad (\text{A1}) \end{aligned}$$

where $Q(\omega, z) \sim n^2(z, T)$ describes the emissivity per unit volume from the electrosphere characterized by the density $n(z, T)$, where z measures the distance from the quark core of the nugget. In Eq. (A1) a complicated function $h(x)$ can be well approximated as

$$h(x) = \begin{cases} 17 - 12 \ln(x/2) & x < 1, \\ 17 + 12 \ln(2) & x \geq 1. \end{cases} \quad (\text{A2})$$

Integrating over ω contributes a factor of $T \int dx (1+x) \exp(-x) h(x) \approx 60 T$, giving the total surface emissivity:

$$F_{\text{tot}} = \frac{dE}{dt dA} = \int_0^\infty d\omega \frac{dF}{d\omega}(\omega) \sim \frac{16}{3} \frac{T^4 \alpha^{5/2}}{\pi} \sqrt[4]{\frac{T}{m}}. \quad (\text{A3})$$

Although a discussion of black-body radiation is inappropriate for these nuggets (for one thing, they are too small to establish thermal equilibrium with low-energy photons), it is still instructive to compare the form of this surface emissivity with that of black-body radiation $F_{BB} = \sigma T^4$:

$$\frac{F_{\text{tot}}}{F_{BB}} \simeq \frac{320}{\pi^3} \alpha^{5/2} \sqrt[4]{\frac{T}{m}}. \quad (\text{A4})$$

At $T = 1 \text{ eV}$ which was an appropriate internal nugget’s temperature for the galactic environment, the emissivity $F_{\text{tot}} \sim 10^{-6} F_{BB}$ is much smaller than that for black-body radiation. As we discuss below a typical internal nugget’s temperature when AQN enters the atmosphere

is of order of $T = 10$ keV which results in the emissivity $F_{\text{tot}} \sim 10^{-5} F_{BB}$ for such high temperatures.

A typical internal temperature of the nuggets can be estimated from the condition the radiative output of equation (A3) must balanced the flux of energy onto the nugget due to the annihilation events. In this case we may write,

$$(4\pi R^2) \frac{16 T^4 \alpha^{5/2}}{3 \pi} \sqrt[4]{\frac{T}{m}} \simeq \kappa (\pi R^2) 2 \text{ GeV} n_{\text{air}} v_{\text{AQN}}, \quad (\text{A5})$$

where the left hand side accounts for the total energy radiation from the nuggets' surface per unit time, while the right hand side accounts for the rate of annihilation events when each successful annihilation event of a single baryon charge produces $\sim 2m_p c^2 \simeq 2 \text{ GeV}$ energy. In Eq. (A5) we assume that the nugget is characterized by the geometrical cross section πR^2 when it propagates in environment with local density n_{air} with velocity $v_{\text{AQN}} \sim 10^{-3} c$.

The factor κ is introduced to account for the fact that not all matter striking the nugget will annihilate and not all of the energy released by an annihilation will be thermalized in the nuggets (e.g. some portion of the energy will be released in form of the axions and neutrinos). As such κ encodes a large number of complex processes including the probability that not all atoms and molecules are capable to penetrate into the colour superconducting phase of the nugget to get annihilated. In a neutral environment when no long range interactions exist the value of κ cannot exceed $\kappa \sim 1$ which would correspond to the total annihilation of all impacting matter into to thermal photons. The high probability of reflection at the sharp quark matter surface lowers the value of κ . The propagation of an ionized (negatively charged) nugget in a highly ionized plasma will increases the effective cross section, and therefore value of κ as discussed in [33] in application to the solar corona heating problem.

Assuming that $\kappa \simeq 1$ one can estimate a typical internal nugget's temperature in the Earth atmosphere:

$$T \sim 40 \text{ keV} \cdot \left(\frac{n_{\text{air}}}{10^{21} \text{ cm}^{-3}} \right)^{\frac{4}{17}} \kappa^{\frac{4}{17}}. \quad (\text{A6})$$

Thus, in the air $T \sim 40 \text{ KeV}$, inside solids $T \sim 200 \text{ KeV}$. There are few additional elements which should be taken into account for Earth's atmosphere in comparison with original computations [29, 30] applied to very dilute galactic environment with much lower temperatures $T \simeq 1\text{eV}$. These effects do not modify the basic scale (A6). However, these additional elements strongly affect the spectrum at the lower frequency bands. In particular the visible portion of the spectrum at $\omega \sim 1\text{eV}$ demonstrates a dramatic suppression. It has some profound consequences for the present work as discussed in the main body of the text. In particular, it implies that the AQNs do not emit the visible light with $\omega \sim 1\text{eV}$, in huge contrast with conventional meteors and meteorites which are normally characterized by strong emission in

the visible frequency bands through sputtering and ablation [38–40].

We start our analysis on additional elements to be implemented with the plasma frequency ω_p which characterizes the propagation of photons in the ionized plasma, which represents the electrosphere for our AQN system. The ω_p can be thought as an effective mass for photon: only photons with the energy larger than this mass can propagate outside of the system, while photons with $\omega < \omega_p$ can only propagate for a short time/distance $\sim \omega_p^{-1}$ before they get absorbed by the plasma. For our estimates we shall use a conventional non-relativistic expression for ω_p :

$$\omega_p^2(z, T) = \frac{4\pi\alpha n(z, T)}{m}, \quad (\text{A7})$$

where the positron density $n(z, T)$ in electrosphere in the nonrelativistic mean-field approximation has been computed in [29, 30]:

$$n(z, T) \simeq \frac{T}{2\pi\alpha} \cdot \frac{1}{(z + \bar{z})^2}, \quad \frac{1}{\bar{z}} \simeq \sqrt{2\pi\alpha m} \sqrt[4]{\frac{T}{m}}, \quad (\text{A8})$$

where \bar{z} is a constant of integration being determined by appropriate boundary condition deep inside the nugget's core. Important implication of the plasma frequency $\omega_p(z, T)$ is that the very dense regions in electrosphere essentially do not emit the photons with $\omega \lesssim \omega_p(z, T)$.

There is another effect which further suppresses the emission of low energy photons. It is related to the ionization processes when the AQN assumes a sufficiently large negative charge due to the $T \neq 0$ as estimated above (A6). Essentially it affects all loosely bound positrons which will be completely stripped off by high temperature, while more strongly bound positrons will be less affected by the same temperature. The corresponding effect leads to very strong suppression of low energy photons with $\omega \ll T$ as loosely bound positrons represent the main source of low frequency photons.

Both these effects have been implemented in Eq. (A1) by performing numerical computation of the integral $\int dz$ over electrosphere region with corresponding modifications of the positron density $n(z, T)$ and inserting $\omega_p(z, T)$ as discussed above. We present the corresponding results for these numerical studies on Fig.4 for $T = 10 \text{ keV}$ and $T = 50 \text{ keV}$. These values for the temperature essentially cover the most relevant window (A6) for the present analysis which dealt with AQN emission in atmosphere.

Few comments are in order. First of all, as one can see from Fig.4 the spectrum is almost flat in the region $\omega \lesssim T$ which is the direct manifestation of the well known soft photon theorem when the emission of the photon with frequency ω is proportional to $d\omega/\omega$. For large $\omega \gg T$ the exponential suppression $\exp(-\omega/T)$ becomes the most important element of the spectrum. The emission is strongly suppressed at very small $\omega \simeq \omega_p \ll T$. The strong suppression of the spectrum with $\omega \ll T$

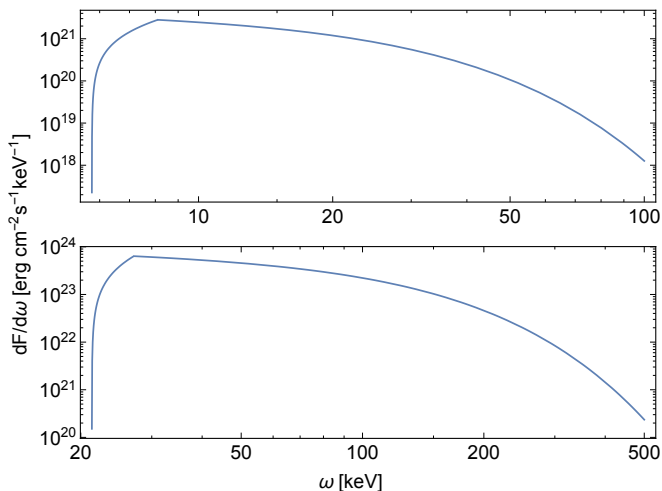


FIG. 4. The spectral surface emissivity of a nugget with the suppression effects at $\omega \ll T$ as discussed in this Appendix. The top plot corresponds to $T = 10$ keV while the bottom plot corresponds to $T = 50$ keV.

has profound phenomenologically consequences: drastic intensity drop at small $\omega \ll T$ implies that the luminosity of the visible light from AQN with $\omega \sim (1 - 10)$ eV is strongly suppressed in comparison with X -ray emission. This strong suppression is entirely due to the two effects mentioned above: the presence of the plasma frequency in electrosphere (A7) and complete stripped off of the loosely bound positrons. It implies that the AQNs cannot be observed by conventional optical monitoring as AQNs are not accompanied by emission of the visible light. It should be contrasted with meteors and meteorites which are normally characterized by strong emission in the visible frequency bands through sputtering and ablation [38–40] and routinely observed by all-sky cameras.

-
- [1] A. R. Zhitnitsky, JCAP **0310**, 010 (2003) [[hep-ph/0202161](#)].
- [2] Skyquake-wikipedia
<https://en.wikipedia.org/wiki/Skyquake>
- [3] Interview with KMVT Chief Meteorologist Brian Neudorff
<https://www.youtube.com/watch?v=JnFZA4Y6Wj4>
- [4] Non-meteoritic event detected by ELFO
http://aquarid.physics.uwo.ca/research/infrasound/is_mysteriousexplosions.html
- [5] Elizabeth A. Silber and Peter G. Brown, Journal of Atmospheric and Solar-Terrestrial Physics, **19**, 116 (2014), <https://doi.org/10.1016/j.jastp.2014.07.005>
- [6] E. Witten, Phys. Rev. D **30**, 272 (1984).
- [7] J. Madsen, Lect. Notes Phys. **516**, 162 (1999) [[astro-ph/9809032](#)].
- [8] R. D. Peccei and H. R. Quinn, Phys. Rev. D **16**, 1791 (1977);
S. Weinberg, Phys. Rev. Lett. **40**, 223 (1978);
F. Wilczek, Phys. Rev. Lett. **40**, 279 (1978).
- [9] J.E. Kim, Phys. Rev. Lett. **43** (1979) 103;
M.A. Shifman, A.I. Vainshtein, and V.I. Zakharov, Nucl. Phys. **B166** (1980) 493(KSVZ-axion).
- [10] M. Dine, W. Fischler, and M. Srednicki, Phys. Lett. **B104** (1981) 199;
A.R. Zhitnitsky, Yad.Fiz. **31** (1980) 497; Sov. J. Nucl. Phys. **31** (1980) 260 (DFSZ-axion).
- [11] K. van Bibber and L. J. Rosenberg, Phys. Today **59N8**, 30 (2006);
- [12] S. J. Asztalos, L. J. Rosenberg, K. van Bibber, P. Sikivie, K. Zioutas, Ann. Rev. Nucl. Part. Sci. **56**, 293-326 (2006).
- [13] Pierre Sikivie, Lect. Notes Phys. **741**, 19 (2008) [[arXiv:0610440v2](#)] [[astro-ph](#)].
- [14] G. G. Raffelt, Lect. Notes Phys. **741**, 51 (2008) [[hep-ph/0611350](#)].
- [15] P. Sikivie, Int. J. Mod. Phys. A **25**, 554 (2010) [[arXiv:0909.0949](#)] [[hep-ph](#)].
- [16] L. J. Rosenberg, Proc. Nat. Acad. Sci. (2015),
- [17] D. J. E. Marsh, Phys. Rept. **643**, 1 (2016) [[arXiv:1510.07633](#)] [[astro-ph.CO](#)].
- [18] P. W. Graham, I. G. Irastorza, S. K. Lamoreaux, A. Lindner and K. A. van Bibber, Ann. Rev. Nucl. Part. Sci. **65**, 485 (2015) [[arXiv:1602.00039](#)] [[hep-ex](#)].
- [19] A. Ringwald, PoS NOW **2016**, 081 (2016) [[arXiv:1612.08933](#)] [[hep-ph](#)].
- [20] I. G. Irastorza and J. Redondo, Prog. Part. Nucl. Phys. **102**, 89 (2018) [[arXiv:1801.08127](#)] [[hep-ph](#)].
- [21] X. Liang and A. Zhitnitsky, Phys. Rev. D **94**, 083502 (2016) [[arXiv:1606.00435](#)] [[hep-ph](#)].
- [22] S. Ge, X. Liang and A. Zhitnitsky, Phys. Rev. D **96**, no. 6, 063514 (2017) [[arXiv:1702.04354](#)] [[hep-ph](#)].
- [23] S. Ge, X. Liang and A. Zhitnitsky, Phys. Rev. D **97**, no. 4, 043008 (2018) [[arXiv:1711.06271](#)] [[hep-ph](#)].
- [24] S. Ge, K. Lawson and A. Zhitnitsky, Phys. Rev. D **99** (2019) no.11, 116017 [[arXiv:1903.05090](#)] [[hep-ph](#)].
- [25] D. H. Oaknin and A. R. Zhitnitsky, Phys. Rev. Lett. **94**, 101301 (2005), [[arXiv:hep-ph/0406146](#)].
- [26] A. Zhitnitsky, Phys. Rev. D **76**, 103518 (2007) [[astro-ph/0607361](#)].
- [27] M. M. Forbes and A. R. Zhitnitsky, JCAP **0801**, 023 (2008) [[astro-ph/0611506](#)].
- [28] K. Lawson and A. R. Zhitnitsky, JCAP **0801**, 022 (2008) [[arXiv:0704.3064](#)] [[astro-ph](#)].
- [29] M. M. Forbes and A. R. Zhitnitsky, Phys. Rev. D **78**, 083505 (2008) [[arXiv:0802.3830](#)] [[astro-ph](#)].
- [30] M. M. Forbes, K. Lawson and A. R. Zhitnitsky, Phys. Rev. D **82**, 083510 (2010) [[arXiv:0910.4541](#)] [[astro-ph.GA](#)].
- [31] V. V. Flambaum and A. R. Zhitnitsky, Phys. Rev. D **99**, no. 2, 023517 (2019) [[arXiv:1811.01965](#)] [[hep-ph](#)].
- [32] A. Zhitnitsky, JCAP **1710**, no. 10, 050 (2017)

- [arXiv:1707.03400 [astro-ph.SR]].
- [33] N. Raza, L. van Waerbeke and A. Zhitnitsky, Phys. Rev. D **98**, no. 10, 103527 (2018) [arXiv:1805.01897 [astro-ph.SR]].
- [34] A. Zhitnitsky, “DAMA/LIBRA annual modulation and Axion Quark Nugget Dark Matter Model,” arXiv:1909.05320 [hep-ph].
- [35] Tommaso Dorigo, few comments on DAMA/LIBRA, posted in Science 2.0 https://www.science20.com/tommaso_dorigo/quark_nuggets_of_dark_matter_as_the_origin_of_damalibra_signal-241740
- [36] K. Lawson, X. Liang, A. Mead, M. S. R. Siddiqui, L. Van Waerbeke and A. Zhitnitsky, Phys. Rev. D **100**, no. 4, 043531 (2019) [arXiv:1905.00022 [astro-ph.CO]].
- [37] E. T. Herrin, D. C. Rosenbaum and V. L. Teplitz, Phys. Rev. D **73**, 043511 (2006) [astro-ph/0505584].
- [38] Elizabeth A. Silber, Mark Boslough, Wayne K. Hocking, Maria Gritsevich, Rodney W. Whitaker, Advances in Space Research, **62**, 489 (2018).
- [39] Elizabeth A. Silber, Peter G. Brown, Journal of Atmospheric and Solar-Terrestrial Physics, **119**, 116 (2014) <https://doi.org/10.1016/j.jastp.2014.07.005>
- [40] Silber, E. A., P. G. Brown, and Z. Krzeminski, J. Geophys. Res. Planets, **120**, 413 (2015) <https://doi.org/10.1002/2014JE004680>
- [41] Douglas ReVelle, J. Geophys. Res. **81**, 1217 (1976) <https://agupubs.onlinelibrary.wiley.com/doi/abs/10.1029/JA081i007p01217>
- [42] M. Tanabashi et al. (Particle Data Group), Phys. Rev. D **98**, 030001 (2018)
- [43] The Elginfield infrasound array (ELFO) http://aquarid.physics.uwo.ca/research/infrasound/is_array.html
- [44] The Elginfield infrasound array (ELFO). The elements. http://aquarid.physics.uwo.ca/research/infrasound/is_elements.html
- [45] ASGARD All-Sky Camera Network <http://aquarid.physics.uwo.ca/research/allsky/overview.html>
- [46] NASA comments on Alabama skyquake https://www.al.com/news/huntsville/2017/11/nasa_still_looking_for_what_ca.html
- [47] Absorption length calculator <http://resource.npl.co.uk/acoustics/techguides/seaabsorption/>
- [48] Tom Parker, Sergey Shatalin1 and Mahmoud Farhadiroushan, *First Break*, volume **32**, 61 (2014)
- [49] T.M. Daley et al, Geophysical Prospecting, **64** 1318 (2016)
- [50] Philippe Jousset et al, Nature Communication, **9** 2509 (2018)
- [51] Jonathan B. Ajo-Franklin et al, Scientific Reports **9** 1328, (2019)
- [52] D. Budker, V. V. Flambaum, X. Liang and A. Zhitnitsky, Phys. Rev. D **101**, no. 4, 043012 (2020) [arXiv:1909.09475 [hep-ph]].
- [53] K. Freese, J. A. Frieman and A. Gould, Phys. Rev. D **37**, 3388 (1988).
- [54] K. Freese, M. Lisanti and C. Savage, Rev. Mod. Phys. **85**, 1561 (2013) [arXiv:1209.3339 [astro-ph.CO]].
- [55] X. Liang, A. Mead, M. S. R. Siddiqui, L. Van Waerbeke and A. Zhitnitsky, Phys. Rev. D **101**, no. 4, 043512 (2020) [arXiv:1908.04675 [astro-ph.CO]].
- [56] Incorporated Research Institutions for Seismology (IRIS) network <https://www.iris.edu/hq/programs/gsn>